ORIGINAL RESEARCH

American Society of Plant Biologists | S-E-B SOCIETY FOR EXPERIMENTAL BIOLOGY | **WILEY**

Asymmetric distribution of extracellular matrix proteins in seed coat epidermal cells of Arabidopsis is determined by polar secretion

Yi-Chen Lee [ID] | Gillian H. Dean [ID] | Erin Gilchrist [ID] | Allen Yi-Lun Tsai [ID] | George W. Haughn [ID]

Department of Botany, University of British Columbia, Vancouver, Canada

Correspondence
George W. Haughn, Department of Botany, University of British Columbia, Vancouver, Canada.
Email: george.haughn@ubc.ca

Present address
Yi-Chen Lee, Biodiversity Research Center, Academia Sinica, Taipei, Taiwan

Erin Gilchrist, Molecular Diagnostics, Anandia Laboratories, Vancouver, Canada

Allen Yi-Lun Tsai, International Research Center for Agricultural & Environmental Biology, Faculty of Advanced Science and Technology, Kumamoto University, Kumamoto, Japan

Abstract

Although asymmetric deposition of the plant extracellular matrix is critical for the normal functioning of many cell types, the molecular mechanisms establishing this asymmetry are not well understood. During differentiation, Arabidopsis seed coat epidermal cells deposit large amounts of pectin-rich mucilage asymmetrically to form an extracellular pocket between the plasma membrane and the outer tangential primary cell wall. At maturity, the mucilage expands on contact with water, ruptures the primary cell wall, and extrudes to encapsulate the seed. In addition to polysaccharides, mucilage contains secreted proteins including the β-galactosidase MUCILAGE MODIFIED 2 (MUM2). A functional chimeric protein where MUM2 was fused translationally with Citrine yellow fluorescent protein (Citrine) indicated that MUM2-Citrine fluorescence preferentially accumulates in the mucilage pocket concomitant with mucilage deposition and rapidly disappears when mucilage synthesis ceases. A secreted form of Citrine, secCitrine, showed a similar pattern of localization when expressed in developing seed coat epidermal cells. This result suggested that both the asymmetric localization and rapid decrease of fluorescence is not unique to MUM2-Citrine and may represent the default pathway for secreted proteins in this cell type. v-SNARE proteins were localized only in the membrane adjacent to the mucilage pocket, supporting the hypothesis that the cellular secretory apparatus is redirected and targets secretion to the outer periclinal apoplast during mucilage synthesis. In addition, mutation of *ECHIDNA*, a gene encoding a TGN-localized protein involved in vesicle targeting, causes misdirection of mucilage, MUM2 and v-SNARE proteins from the apoplast/plasma membrane to the vacuole/tonoplast. Western blot analyses suggested that the disappearance of MUM2-Citrine fluorescence at the end of mucilage synthesis is due to protein degradation and because several proteases have been identified in extruded seed mucilage. However, as mutation of these genes did not result in a substantial delay in MUM2-Citrine degradation and the

timing of their expression and/or their intracellular localization were not consistent with a role in MUM2-Citrine disappearance, the mechanism underlying the abrupt decrease of MUM2-Citrine remains unclear.

Highlight

Extracellular matrix proteins in Arabidopsis seed coat epidermal cells exhibit distinctive asymmetric distributions. We show that this pattern is generated by polar secretion and protein degradation.

KEYWORDS

Arabidopsis, asymmetric distribution, cell wall, extracellular matrix, mucilage, polar secretion, proteases, seed coat

1 | INTRODUCTION

Plant cells are surrounded by an extracellular matrix composed of a variety of complex organic molecules including polysaccharides, glycoproteins, polyphenols, and lipids. Like many other parts of the cell, components of the extracellular matrix are often deposited and distributed asymmetrically, and this asymmetry is important for cell development, structure, and function. For example, cells that elongate asymmetrically via tip growth, such as pollen tubes and root hairs, deposit cell wall material primarily at the elongating tip and with a composition that allows flexibility during growth while reinforcing the sides of the elongating tube with cellulose (Rounds & Bezanilla, 2013). Similarly, differentiating epidermal cells deposit cuticular material into the extracellular matrix only on the side of the cell facing the external environment (Samuels et al., 2008) and differentiating tracheary elements deposit cellulose, lignin, and xylan in complex patterns (Schuetz et al., 2013).

Much of the available knowledge concerning mechanisms underlying the asymmetric deposition of extracellular matrix has come from studies of cells showing asymmetries in growth and division including pollen tubes, root hairs, moss protonema, leaf pavement cells, and stomata (reviewed in Rounds & Bezanilla, 2013; Qi & Greb, 2017; Yang et al., 2020). In general, an asymmetrically distributed extrinsic signal activates a signal transduction pathway involving a receptor-like kinase that leads to polarization in the plasma membrane and activation of small, plant, Rho-like guanine triphosphate hydrolases (Rho of Plants or ROP). ROPs influence secretion, partly through a rearrangement of the cytoskeleton, such that secretory vesicles carrying extracellular matrix or proteins that modify the matrix are targeted to a specific domain of the plasma membrane (Bove et al., 2008; Kost, 2008; Lancelle & Hepler, 1992; Yalovsky et al., 2008).

Despite the progress toward understanding the establishment of cell polarity, significant gaps in our knowledge about the asymmetric deposition of the extracellular matrix remain. For example, the extrinsic signals that initiate the process are largely unknown and a description of subsequent steps in signal transduction in any single cell type is fragmentary. At least part of the problem arises from the fact that current model cell types manifest polarity through asymmetric growth and/or division, complex processes that depend on a relatively large number of cellular events. In addition, asymmetric deposition of extracellular matrix in cells that no longer grow and divide may involve distinct mechanisms. For both of these reasons, the investigation of differentiating cells that distribute their extracellular matrix asymmetrically independent of cell growth could provide valuable new information about cell polarity.

The seed coat epidermal cells of *Arabidopsis thaliana* (Arabidopsis) have a highly polarized extracellular matrix, with large amounts of pectin-rich mucilage (mainly composed of rhamnogalacturonan-I, RG-I) deposited asymmetrically, resulting in a donut-shaped pocket between the primary cell wall and a thick volcano-shaped secondary cell wall (columella) on the outer periclinal side of the cells (reviewed in Šola, Dean, & Haughn, 2019). During seed development, the accumulation of mucilage in the apoplast begins after the cessation of cell growth at approximately 5 days post anthesis (DPA) and finishes prior to 9 DPA (Beeckman et al., 2000; Western et al., 2000; Windsor et al., 2000; Young et al., 2008). During this period, mucilage components are initially deposited at the junction of the radial and outer periclinal cell walls. Accumulation of mucilage between the wall and the plasma membrane results in expansion of the donut-shaped pocket. Concomitantly, the large central vacuole contracts toward the inner periclinal side of the cell leaving a volcano-shaped column of cytoplasm (cytoplasmic column). At approximately 8 DPA mucilage deposition ends and synthesis of cellulose along the plasma membrane lining of the mucilage pocket to form the columella is initiated. As the columella increases in size, the cytoplasm contracts toward the bottom of the cell. By maturity, the space formerly occupied by the cytoplasm is entirely replaced by the columella. When mature, dry seeds are hydrated, and the mucilage extrudes to form a gelatinous halo around the seed.

The Arabidopsis seed coat epidermal cell is an attractive model for the investigation of mechanisms underlying the asymmetric deposition of extracellular matrix for several reasons. First, the spatial and temporal events during cellular differentiation of this cell type have been characterized. Second, the pattern of extracellular matrix

distribution is distinctly asymmetric but relatively simple. Third, extracellular matrix asymmetry occurs after the cessation of cell growth and is the primary process that drives continued cell differentiation. Finally, seed coat epidermal cells are amenable to cellular, biochemical, and as a nonessential cell type, genetic manipulation (Haughn & Western, 2012).

All available evidence suggests that asymmetry of the extracellular matrix in Arabidopsis seed coat epidermal cells is established by polar secretion of matrix polysaccharides and the enzymes that modify them. RG-I, the major polysaccharide of Arabidopsis seed mucilage, has been detected in the Golgi apparatus and secretory vesicles and accumulates in the mucilage pocket during mucilage synthesis in seed coat epidermal cells (Young et al., 2008). All proteins known to be secreted to the apoplast during seed mucilage synthesis that have been investigated to date are concentrated in the mucilage pocket, for example, MUCILAGE MODIFIED 2 (MUM2; Shi et al., 2019), PEROXIDASE 50 (PRX50; Francoz et al., 2019), and TESTA ABUNDANT 1 (TBA1), TBA2, and TBA3 (Tsai et al., 2017), the plasma membrane, for example, CELLULOSE SYNTHASE A5 (CESA5), CESA3, and CESA10 (Griffiths et al., 2015), or a portion of the primary wall surrounding the pocket, for example, PEROXIDASE36 (PER36; Kunieda et al., 2013).

The MUM2 protein is a ß-galactosidase that is produced by seed coat epidermal cells during mucilage synthesis (Dean et al., 2007; Macquet et al., 2007; Šola, Gilchrist, et al., 2019). MUM2 is secreted into the mucilage pocket where it removes galactose side-chains from RG-I. Loss-of-function mutation of *MUM2* results in mucilage that cannot extrude when mature, dry seeds are hydrated. Since MUM2 is secreted primarily to the mucilage pocket and has RG-I as its substrate, we investigated the spatial and temporal pattern of MUM2 localization in seed coat epidermal cells using a Citrine Yellow Fluorescent Protein (Citrine) tag, and examined the effect on that localization of a mutant allele of *ECHIDNA*, a gene encoding a Trans Golgi Network (TGN) protein required for correct intracellular targeting of mucilage. We show that the asymmetric distribution of MUM2 does not depend on its amino acid sequence. Rather, the differentiating cells seem to target all cargo destined for the apoplast to the mucilage pocket. In addition, we demonstrate that the MUM2-Citrine polypeptide and the fluorescence of the Citrine disappears rapidly following the completion of mucilage synthesis. The mechanism underlying this apparent protein degradation, however, remains elusive.

2 | MATERIAL AND METHODS

2.1 | Plant materials and growth conditions

Mutant seeds from the SALK (Alonso et al., 2003), SAIL (Sessions et al., 2002), and GABI-Kat (Kleinboelting et al., 2012) T-DNA insertion collections were obtained from the Arabidopsis Biological Resource Center (ABRC; abrc.osu.edu). Accession numbers for mutant lines are included in the Supporting Information. *mum2-1* was

generated previously in our lab (Western et al., 2001). Seeds of $P_{AtVAMP721}$::mRFP-VAMP721 and $P_{AtVAMP722}$::mRFP-VAMP722 transgenic plants were kindly provided by Professor Masa H. Sato (Ichikawa et al., 2014).

Seeds were germinated on petri plates containing an agar minimal medium designed for *A. thaliana* (Haughn & Somerville, 1986; referred to as AT medium) in growth chambers at 20°C under continuous light (90–120 μmol m^{-2} s^{-1} photosynthetically active radiation, PAR). Ten-day-old seedlings were transplanted to soil (Sunshine 4 mix, Sun Gro Horticulture), watered once with liquid AT medium, and grown under the same conditions.

2.2 | Constructs and transgenic plants

Constructs for localization of proteins fused to Citrine YFP (Citrine) were generated using the pAD vector (DeBono, 2011) using restriction endonucleases and standard molecular cloning techniques. Constructs for determining the localization of proteins fused to mRFP were generated using the Gateway cloning system and following the manufacturers protocols (Thermo Fisher Scientific). Protein-mRFP fusions under control of their own promoter were assembled in the Gateway destination vector pGWB553 (Nakagawa et al., 2009), whereas protein-mRFP fusions under control of the seed coat-specific TBA2 promoter (McGee et al., 2019; Tsai et al., 2017) were assembled using MultiSite Gateway technology in the destination vector R4pGWB553 (Nakagawa et al., 2008; Oshima et al., 2011). Full details of the cloning including primer sequences are given in the Supporting Information. Constructs were verified by sequencing before being introduced into *Agrobacterium tumefaciens* GV3101 (pMP90) and transformed into plants using the floral spray method (Chung et al., 2000). For constructs generated in the pAD binary vector, pSoup plasmid was co-transformed (Hellens et al., 2000). T1 seeds were selected on AT medium plates containing the appropriate antibiotics.

2.3 | Genotyping

DNA from mutant and transgenic lines was collected on Whatman FTA cards (Sigma-Aldrich) for PCR genotyping using primers listed in the Supporting Information. For *mum2-1*, PCR product was digested with *Tat*I restriction enzyme (Thermo Fisher Scientific) after amplification. The *mum2-1* PCR product is cleaved whereas the wild type product is not.

2.4 | SDS-PAGE and immunoblot analysis

Developing siliques were staged according to Western et al. (2000). Several seeds were removed from a single silique at the required time point and examined using fluorescence microscopy using an Axioskop 2 light microscope (Carl Zeiss) equipped with a CCD camera (DFC450 C; Leica) and LAS software (v4.2.0; Leica) to determine MUM2-Citrine

fluorescence pattern. The remainder of the seeds from the same silique were harvested, frozen on dry ice, and stored at −80°C in 1.5-ml microcentrifuge tubes until needed. Frozen tissue was homogenized in the microfuge tube using a micropestle and 40 μl of extraction buffer (Lu et al., 2010); 10 μl of 5× SDS-PAGE load dye (225-mM Tris pH 6.8, 50% [v/v] glycerol, 10% [w/v] SDS, 0.25-M DTT, 0.05% Bromophenol Blue) was added, and the samples vortexed before being denatured at 95°C for 10 min. Cellular debris was removed by centrifugation at $12000 \times g$ for 10 min before the supernatant was transferred to a new tube. The entire protein sample was loaded and separated by SDS-PAGE on 10% gel (Laemmli, 1970) before being transferred to nitrocellulose membrane by semidry electroblotting using Bjerrum Schafer-Nielsen buffer with SDS (48-mM Tris, 39-mM glycine, 20% methanol, 1.3-mM SDS, pH 9.2). Membranes were blocked with 5% skim milk powder in TBS-T buffer (150-mM NaCl, 10-mM Tris, pH 8.0, 0.1% Tween 20) for 30 min at room temperature (RT) on an orbital shaker at 60 rpm. Anti-GFP antibody (mouse, cat# 11814460001, Roche) diluted to 1:10,000 in TBS-T buffer was then incubated with the membrane overnight at 4°C at 60 rpm. HRP-conjugated anti-mouse IgG secondary antibody (cat# A16066, Thermo Fisher Scientific) diluted to 1:20,000 with TBS-T buffer was used to detect anti-GFP, and peroxidase activity was detected with UltraScence Western Substrate (cat# CCH365_Femto, FroggaBio). Blots were the stripped by washing twice for 10 min each in mild stripping buffer (200-mM glycine, .1% SDS (w/v), 1% Tween 20 (w/v), pH 2.2), then twice for 10 min each in PBS pH 7.0, then twice for 5 min each in TBS-T (protocol at babcam.com) before being blocked and re-probed as described above using antitubulin primary antibody (mouse, cat# T5168, Sigma-Aldrich) and the same secondary antibody.

2.5 | Ruthenium red staining and calcofluor staining of mature seeds

To stain mature seeds without shaking, seeds were hydrated in water and left to stand for 15 min before the water was replaced with 0.02% (w/v) ruthenium red (cat# 00541, Sigma-Aldrich). Seeds were then left to stand for a further 15 min. To stain seeds with shaking, seeds were hydrated in water for 1 h at 130 rpm on an orbital shaker before the water was replaced with 0.01% ruthenium red and the seeds stained for 1 h at 130 rpm. After staining, the ruthenium red solution was removed and seeds rinsed and mounted in water, then viewed using an Axioskop 2 light microscope (Carl Zeiss) equipped with a CCD camera (DFC450 C; Leica) and LAS software (v4.2.0; Leica). The area of seeds and mucilage halos were measured using Photoshop and statistical analysis was performed using R.

To stain mature seeds with calcofluor (calcofluor white M2R; cat# F3543, Sigma-Aldrich), mature seeds were hydrated in water for 2 h with head over tail rotation, and then stained with .02% (w/v) calcofluor white for 1 h. After staining, the calcofluor solution was removed before seeds were rinsed and mounted in water, then viewed using an UltraView VoX spinning disk confocal microscope

(PerkinElmer) equipped with an EMCCD camera (C9100-02; Hamamatsu) and Volocity software (Improvision). Signal was examined using a 405 nm excitation laser and 460/50 nm emission filter.

Microscope images were processed using Photoshop (Adobe Photosystems) and Inkscape (inkscape.org).

2.6 | Live cell fluorescent confocal microscopy

Confocal microscopy was performed using an UltraView VoX spinning disk confocal microscope (PerkinElmer) equipped with an EMCCD camera (C9100-02; Hamamatsu) and Volocity software (Improvision). Citrine signal was examined with a 514-nm excitation laser and 540/30 nm emission filter, and mRFP signal was examined with a 561-nm excitation laser and 595/50 nm emission filter. Microscope settings were the same for all images acquired within the same experiment.

Developing seed was stained with FM4-64 (cat# T13320, Thermo Fisher Scientific) by removing seeds from siliques and immersing in 10-μM FM4-64 in water. Seeds were vacuum infiltrated for 5 min, then left to stain for 10 min before imaging. Other tissues were stained with 10-μM FM4-64 for 5 min without applying a vacuum before imaging using a 561-nm excitation laser and 650/75 nm emission filter.

Microscope images were processed with ImageJ (Schindelin et al., 2012), Photoshop (Adobe Photosystems) and Inkscape (inkscape.org). All images are single optical slices rather than flattened Z stacks.

2.7 | Accession numbers

Sequence data from this article can be found in the GenBank/European Molecular Biology Laboratory databases under the following accession numbers: *MUM2* (At5g63800), *ECHIDNA* (At1g09330), *ASPG1* (At3g18490), *RD21A* (At1g47128), *SCPL35* (At5g08260), *ARA12* (At5g67360), *VAMP721* (At1g04750), *VAMP722* (At2g33120).

3 | RESULTS

3.1 | MUM2 is distributed in a polar manner in seed coat epidermal cells but not in other tissues

To determine the spatiotemporal distribution of MUM2 relative to its seed mucilage substrate RG-I, genomic *MUM2* sequence including the coding region, introns and 2 kb upstream of the start codon was fused with *Citrine* yellow fluorescent protein (*gMUM2-Citrine*). *gMUM2-Citrine* was introduced into the *mum2-1* mutant and shown to complement the *mum2* mucilage extrusion phenotype (Figure S1A–C), indicating that the fusion protein was functional in the seed coat. Seed coat development was staged by marking the pedicel of flowers on the day they open (0 days post anthesis, DPA).

The localization of MUM2-Citrine fluorescence in the seed coat epidermal cells from 4 DPA to 10 DPA was examined using confocal microscopy. No MUM2-Citrine signal was detected at 4 DPA (data not shown). MUM2-Citrine was first observed at 5 DPA and was located in the primary wall (Figure 1a,g). The strongest fluorescence was observed where the radial and outer periclinal walls meet (the position of the future mucilage pocket, Figure 1g, arrowhead), with lower fluorescence in the remainder of the primary cell wall. From 6 DPA to 8 DPA, during the period of mucilage deposition, MUM2-Citrine fluorescence was found primarily in the mucilage pocket (Figure 1b–d,h–j). To ensure that the MUM2-Citrine fluorescence was in the apoplast, the cells were counterstained with the membrane dye FM4-64. MUM2-Citrine was located between the membrane and the cell wall, indicating that MUM2-Citrine is indeed secreted to the apoplast (Figure S1E–G). Following the completion of mucilage synthesis, the MUM2-Citrine signal abruptly disappeared from the mucilage pocket (9 DPA) but continued to accumulate in the developing columella (Figure 1e,k). The MUM2-Citrine signal in the columella was still detectable at 10 DPA (Figure 1f,l) but gradually decreased after this point in time. Therefore, the secretion of MUM2 appears to be polar and coincident, temporally and spatially, with its

mucilage substrate during seed coat epidermal cell differentiation (Young et al., 2008). In addition, these data raise the possibility that MUM2 is actively removed at the end of mucilage synthesis.

MUM2 is expressed in a wide variety of cell types (Dean et al., 2007; Macquet et al., 2007). To check if the polar distribution is unique to seed coat epidermal cells, the distribution pattern of MUM2-Citrine was examined in other tissues. MUM2-Citrine fluorescence is present in the epidermal cells of the cotyledons in 7-day-old seedlings (Figure 1m) and in the leaves of 14-day-old seedlings (Figure 1n) and is distributed in a nonpolar manner in these tissues. In 7-day-old seedlings, MUM2-Citrine fluorescence is detected in epidermal cells of the root elongation zone but not in the root tip (Figure 1o). In the mature root, fluorescence was detected in the epidermis including root hairs and in cortex cells (Figure 1p). To confirm apoplastic localization of MUM2-Citrine, root tissue was counterstained with the plasma membrane dye FM4-64. MUM2-Citrine signal was detected between the plasma membranes of adjoining cells, indicating that MUM2-Citrine is located in the apoplast (Figure S1H–J). Given that MUM2-Citrine is distributed in an asymmetric manner only in seed coat epidermal cells, these data suggest that the polar localization is a characteristic of this specialized cell type.
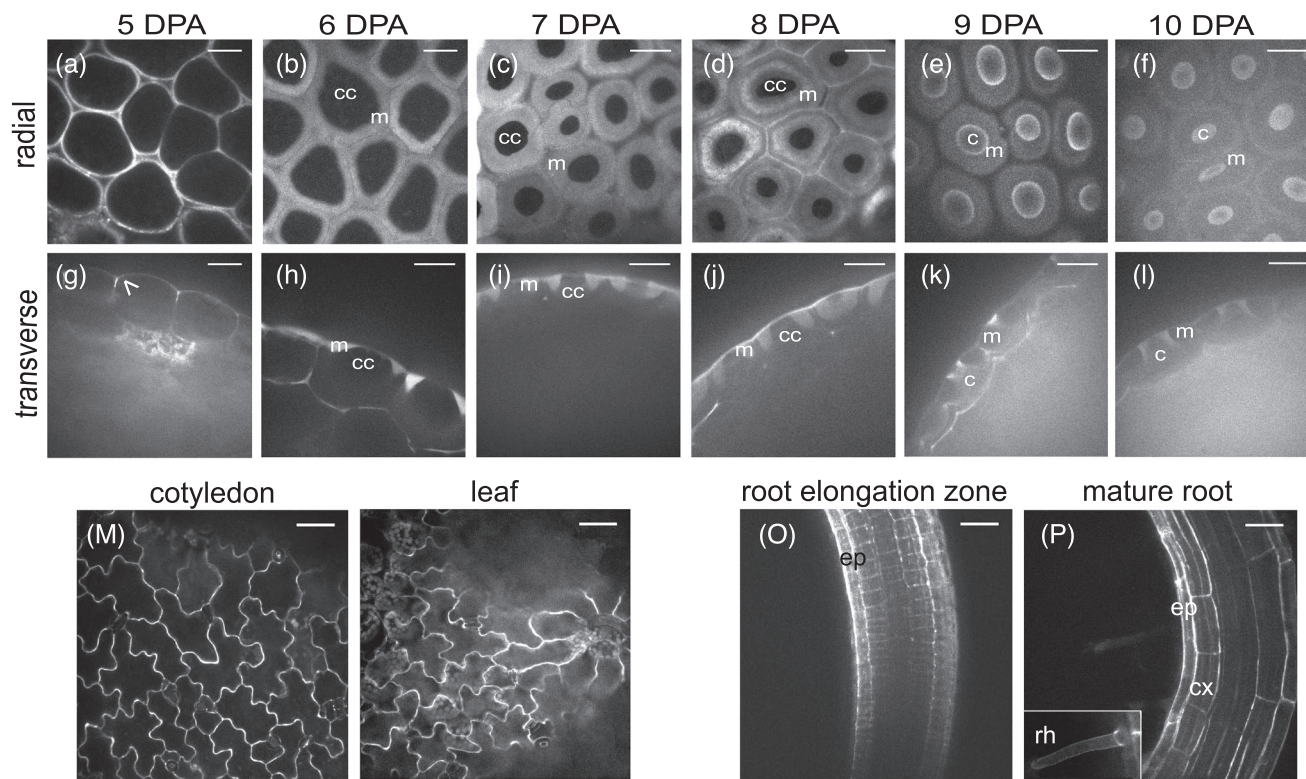

FIGURE 1   Distribution pattern of gMUM2-Citrine. (a–l) Radial (a–f, top panels) and transverse (g–l, bottom panels) confocal images of developing seed coat epidermal cells at 5 (a,g), 6 (b,h), 7 (c,i), 8 (d,j), 9 (e,k), and 10 (f,l) DPA. At 5 DPA, gMUM-Citrine signal is observed at the site of mucilage accumulation where the radial wall meets the outer periclinal wall (g, arrowhead). At 6–8 DPA, the fluorescence is seen in the mucilage pocket (b–d,h–j). At 9 and 10 DPA, fluorescence disappears from the mucilage pocket but can be seen in the newly synthesized secondary cell wall of the columella (e,f,k,l). (m,n) gMUM-Citrine distribution is not polar in the apoplast of cotyledon (m) and leaf (n) epidermal cells in seedlings 7 days after germination. (o,p) In the roots of seedlings 7 days after germination, gMUM2-Citrine fluorescence is visible in the epidermal cells of the elongation zone (o). In the mature root (p) signal is present in the cortex and epidermis, including root hairs (p, inset). Scale bars 20 μm (a–l) or 50 μm (m–p). c, columella; cc, cytoplasmic column; m, mucilage pocket; cx, cortex; ep, epidermis; r, root hair

3.2 | Targeting of secretion to the mucilage pocket is not dependent on the sequence of the secreted protein

To investigate whether the polar distribution of MUM2-Citrine is determined by its amino acid sequence, we generated two secretory forms of Citrine by fusing either the predicted 28 amino acid signal sequence from *MUM2* (*MUM2SP-Citrine*; SignalP-5.0 Server, www.cbs.dtu.dk/services/SignalP; Armenteros et al., 2019) or the signal sequence from an Arabidopsis chitinase gene in-frame with Citrine (*secCitrine*; Batoko et al., 2000; McGee et al., 2021). These chimeric genes were placed under the control of a 1.5-kb fragment of the Arabidopsis *MUM4* promoter that drives expression in seed coats between 4 and 10 DPA with highest expression at 6–7 DPA (*MUM4pro1.5*, includes the 5′ UTR; Dean et al., 2017). In addition, a positive control consisting of the *MUM2* cDNA fused in-frame to *Citrine* (*cMUM2-Citrine*) and a negative control comprising the *Citrine* coding sequence without a signal peptide (*cytoCitrine*) were also placed under the control of *MUM4pro1.5*. *MUM2SP-Citrine*, *secCitrine*, *cytoCitrine*, and an empty pAD vector control were individually transformed into wild type Col-2 Arabidopsis. *cMUM2-Citrine* was introduced into the *mum2* and complementation was confirmed (Figure S1A–D). The localization of Citrine fluorescence in 7 DPA developing seed coat epidermal cells was examined using confocal microscopy. The localization of cMUM2-Citrine (Figure 2a,e) was largely indistinguishable from the asymmetric distribution of gMUM2-Citrine described above (Figure 1c,i), indicating that using the *MUM4* rather than the *MUM2* promoter did not influence protein distribution. Interestingly, both secCitrine (Figure 2b,f) and MUM2SP-Citrine (Figure 2c,g) also appeared primarily in the mucilage pocket. Since MUM2 and secCitrine proteins do not share any significant amino acid sequence similarity, it is unlikely that their polar distribution in seed coat epidermal cells is determined primarily by their primary amino acid sequence. As expected, the fluorescence signal of cytoCitrine was observed only in the cytoplasm and not the apoplast (Figure 2d,h), and no fluorescence signal was detected in transgenic plants carrying pAD (data not shown).

3.3 | The secretory pathway appears to be directed to the mucilage pocket in seed coat epidermal cells

The observations that MUM2 is distributed uniformly in the apoplast of cells other than the seed coat epidermis, and the polar localization of proteins in seed coat epidermal cells appears to be independent of a specific amino acid sequence suggests that polar secretion is the default pathway in seed coat epidermal cells during differentiation. Vesicle-associated membrane proteins (VAMPs), members of the v-SNARE protein family, facilitate fusion of vesicles to a target membrane (Sanderfoot et al., 2000; Uemura et al., 2004). As well as being localized to vesicles, VAMPs are observed in the target membrane following vesicle fusion (Dittman & Kaplan, 2006). Using seed coat microarray data (Dean et al., 2011), we identified two VAMP genes, VAMP721 and 722, which are expressed in developing Arabidopsis seed coat cells and have been shown to accumulate asymmetrically in
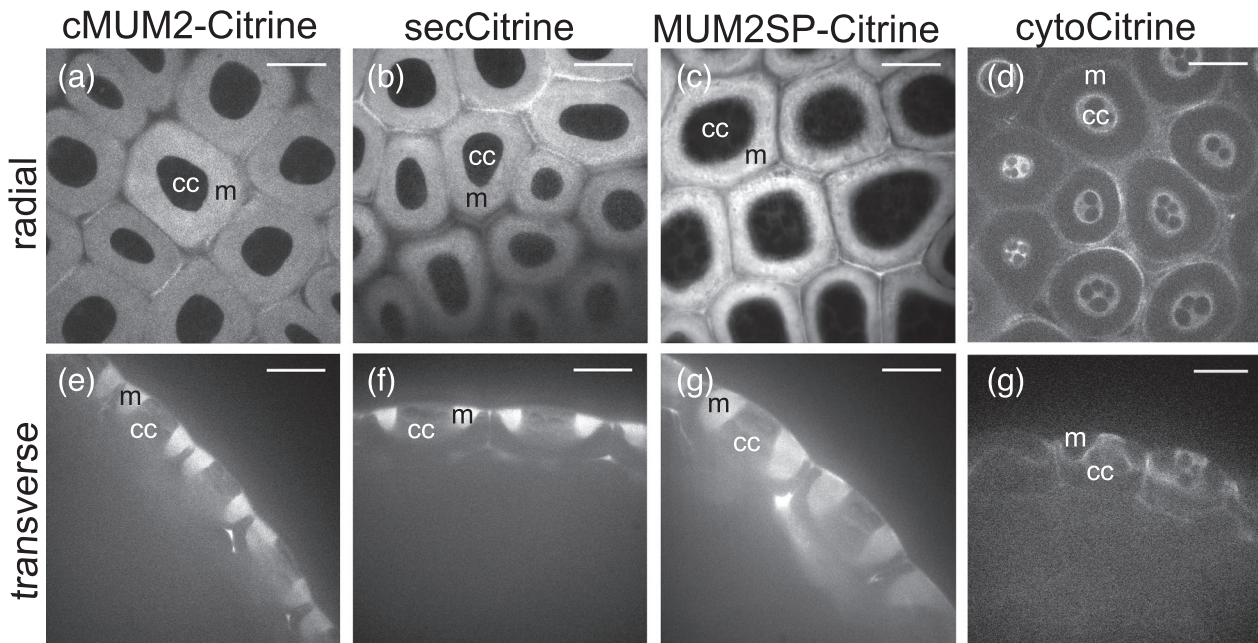

FIGURE 2 Polar secretion of Citrine-tagged proteins in seed coat epidermal cells. (a–h) Radial (a–d, top panels) and transverse (e–h, bottom panels) confocal images of developing seed coat cells at 7 DPA. cMUM2-Citrine (a,e), secCitrine (b,f), and MUM2SP-Citrine (c,g) fluorescence is located in the mucilage pocket. Conversely, cytoCitrine (d,h) is located in the cytoplasmic column. Scale bars = 20 μm. cc, cytoplasmic column; m, mucilage pocket

the plasma membrane and act redundantly in response to pathogen attack (Kwon et al., 2008) and at the tip of elongating root hairs (Ichikawa et al., 2014). To investigate whether vesicle trafficking to the plasma membrane is polarized in seed coat epidermal cells, we obtained transgenic lines carrying monomeric red fluorescence protein (mRFP) translationally fused to the N-terminus of VAMP721 and VAMP722 under the control of their own promoters (Ichikawa et al., 2014) and examined their distribution.

Both mRFP-VAMP721 and mRFP-VAMP722 fluorescence were distributed in a punctate pattern around the entire circumference of the cell membrane at 4 DPA (Figure 3a,g) but by 5 DPA was localized primarily in the membrane along the radial wall and at the outer corner of the cell (Figure 3b,h; arrowhead). During mucilage secretion between 6 and 8 DPA, mRFP-VAMP721 and mRFP-VAMP722 signal was located primarily along the membrane lining the mucilage pocket (Figure 3c–e,i–k). By 9 DPA, when mucilage secretion is complete, mRFP-VAMP721 and mRFP-VAMP722 fluorescence was no longer detected in the plasma membrane (Figure 3f,l). The change in mRFP-VAMP721 and mRFP-VAMP722 distribution in the plasma membrane from relatively uniform to an increased concentration at the mucilage pocket during mucilage secretion suggests that the secretory pathway shifts from being relatively untargeted to being polar during seed coat epidermal cell differentiation and results in the delivery of mucilage-related proteins and polysaccharides to a specific domain of the apoplast.

Because the distribution of mRFP-VAMP721 and mRFP-VAMP722 in the plasma membrane correlates with both mucilage polysaccharide and MUM2-Citrine localization in the apoplast, these VAMPs may be required for their secretion. As decreased secretion of either mucilage polysaccharide or MUM2-Citrine should impair mucilage release from mature seeds, we examined mucilage extrusion in vamp721 and vamp722 single mutants. However, no obvious differences compared to wild type were observed when seeds were shaken in water and stained with ruthenium red (data not shown). The function of VAMP721 and VAMP722 is known to be redundant and the vamp721vamp722 double mutant is seedling lethal (Zhang et al., 2011), making it impossible to determine their effect on seed coat development directly. To investigate whether lines that were homozygous mutant for one locus and heterozygous for the second would be viable but show a mucilage extrusion phenotype, both vamp721(−/+)722(−/−) and vamp721(−/−)722(−/+) lines were generated. Although both lines were viable, when compared to wild type, neither showed defects in mucilage extrusion when seeds were hydrated by shaking in water for 2 h and then stained with ruthenium red (Figure 3m–o).

3.4 | VAMP721 localization, and secretion of MUM2 and mucilage polysaccharides, are mediated by the Trans Golgi Network protein ECHIDNA

ECHIDNA (ECH) is a Trans Golgi Network (TGN)-localized protein involved in vesicle targeting but not endocytosis (Gendre et al., 2011).

It has been shown that the majority of mucilage is mistargeted to the vacuole in ech mutants (Gendre et al., 2013; McFarlane et al., 2013). Interestingly, secreted plasma membrane proteins such as the ABC transporter G family member ABCG11 and plasma membrane intrinsic protein PIP2 accumulate in a different location to mucilage polysaccharides, indicating that although these cargos are destined for the plasma membrane they may be secreted via distinct pathways (McFarlane et al., 2013).

To test if the secretion of MUM2 is also dependent on ECH, gMUM2-Citrine was crossed into the ech mutant background and the distribution of Citrine fluorescence in seed coat epidermal cells determined by confocal microscopy. Like mucilage polysaccharide, MUM2-Citrine signal was found primarily in the vacuole as well as in the small mucilage pockets of the ech seed coat epidermal cells (Figure 3p,q), indicating that the secretion of both mucilage polysaccharide and MUM2 is controlled by an ECH-dependent pathway.

Since the distribution pattern of mRFP-VAMP721 in the plasma membrane matches the site of MUM2-Citrine and mucilage polysaccharide secretion in seed coat epidermal cells, we crossed mRFP-VAMP721 into the ech background to test if the mRFP-VAMP721-carrying vesicles are mis-targeted. mRFP-VAMP721 was found in the tonoplast of 7 DPA seed coat epidermal cells in the ech mutant (Figure 3r,s), indicating that targeting of VAMP721 to the mucilage pocket also requires ECH. Further, the mis-localization pattern of mRFP-VAMP721 in ech matches that of mucilage polysaccharide and MUM2-Citrine, consistent with the hypothesis that MUM2 and mucilage polysaccharide are secreted through VAMP721-carrying vesicles.

3.5 | Disappearance of MUM2-citrine fluorescence in the mucilage pocket at 9 DPA is correlated with decreased MUM-citrine protein

The secretion of seed mucilage ends by 9 DPA (Young et al., 2008) and at this time, the fluorescence of MUM2-Citrine disappears abruptly from the mucilage pocket (Figure 1). This disappearance could be due to protein degradation or changes in the chemical environment that result in quenching of the Citrine fluorescence. To distinguish between these possibilities, western blot analysis was used to assess MUM2-Citrine protein levels during seed development.

Disappearance of Citrine fluorescence happens in a relatively short period of time, and staging of seed coats by marking open flowers has some unavoidable inaccuracy due to variation in the exact structure of the inflorescence. Therefore, we examined 7, 8, 9, and 10 DPA developing seeds using fluorescence microscopy to determine the location of MUM2-Citrine, and then performed western blots on the same isolated seeds (Figure 4a). MUM2-Citrine fluorescence was detected in the mucilage pocket at 7 and 8 DPA. At 9 and 10 DPA, fluorescence was absent in the mucilage pocket but was observed in the developing secondary cell wall (columellae). Total protein was then extracted from these seeds and used to prepare western blots. The blot was first probed with anti-GFP antibody, which
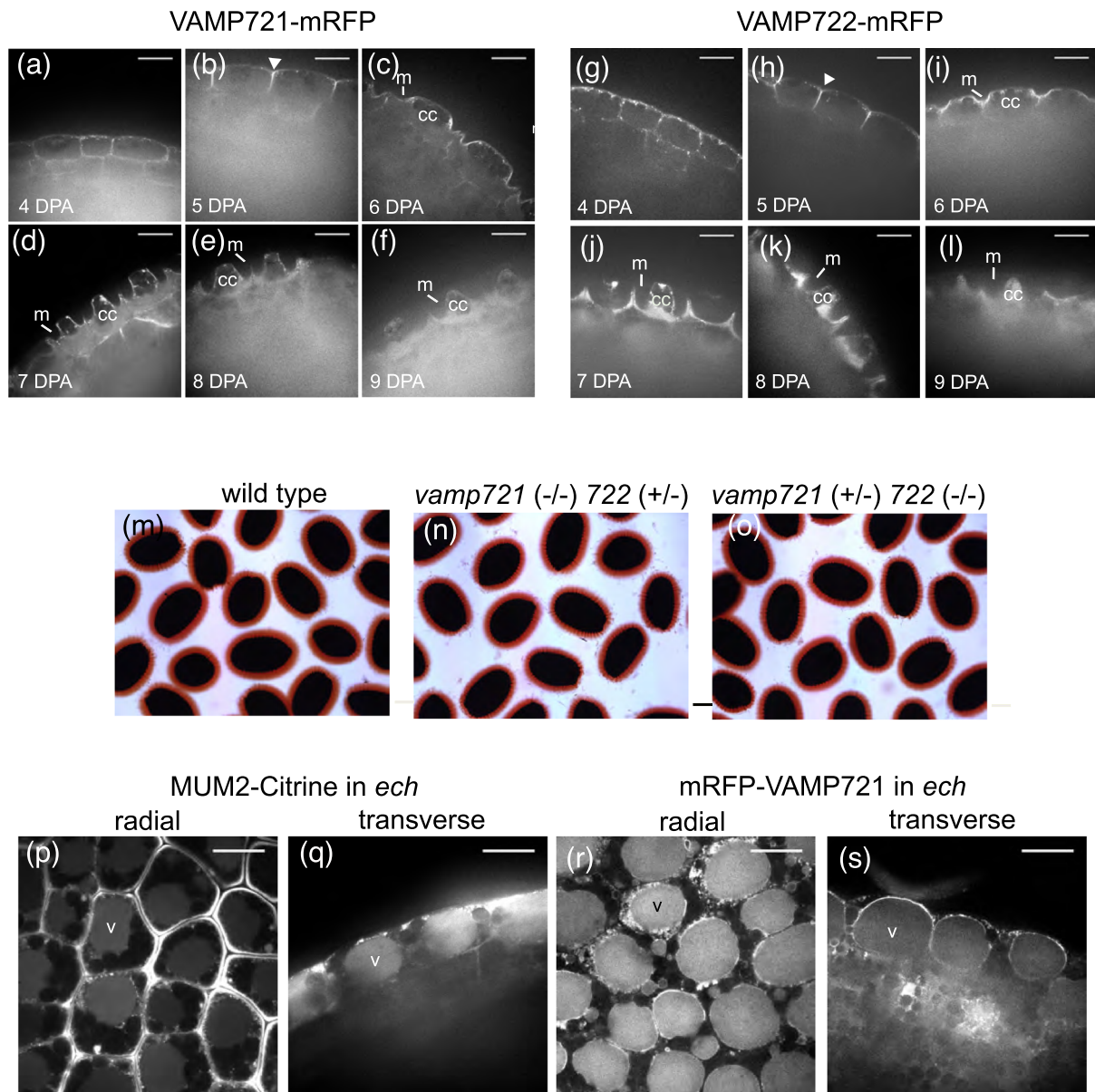
VAMP721-mRFP

VAMP722-mRFP

wild type   *vamp721 (-/-) 722 (+/-)*   *vamp721 (+/-) 722 (-/-)*

MUM2-Citrine in *ech*
radial   transverse

mRFP-VAMP721 in *ech*
radial   transverse

FIGURE 3 The targeting of vSNARE proteins VAMP721 and VAMP722 to the plasma membrane lining the mucilage pocket in seed coat epidermal cells requires the function of the ECHIDNA protein. (a–f) Transverse images of seed coat epidermal cells at 4 (a,g), 5 (b,h), 6 (c,i), 7 (d,j), 8 (e,k), and 9 (f,l) DPA showing fluorescent signal from VAMP721-mRFP and VAMP722-mRFP obtained using confocal microscopy. At 4 DPA, signal is distributed evenly around the cell (a,g). By 5 DPA, signal accumulates at the future site of mucilage secretion where the radial wall meets the outer periclinal wall (b,h; arrowhead). When mucilage is being actively secreted at 6–8 DPA, VAMP721-mRFP and VAMP722-mRFP fluorescence is located along the plasma membrane that lines the mucilage pocket (c–e,i–k) but disappears after mucilage secretion ends at 9 DPA (f,l). (m–o) Mucilage phenotypes of wild type (m), *vamp721(−/−)722(+/−)* (n), and *vamp721(−/+)722(−/−)* (o) determined by shaking seed in water for 15 min before extruded mucilage was stained with ruthenium red. No obvious mucilage extrusion defect was identified in *vamp721(−/−)722(+/−)* (N) or *vamp721(−/+)722(−/−)* (o). (p–s) Distribution of MUM2-Citrine (p,q) and mRFP-VAMP721 (r,s) fluorescence in 7 DPA seed coat epidermal cells of the *ech* mutant was examined using confocal microscopy. MUM2-Citrine fluorescence was identified in the vacuole in both radial (p) and transverse (q) optical sections, while mRFP-VAMP721 fluorescence lined the tonoplast in radial (r) and transverse (s) sections. Scale bars = 20 μm (a–l and p–s) or 200 μm (m–o). cc, cytoplasmic column; m, mucilage pocket; v, vacuole

detects full length MUM2-Citrine protein (∼120 kDa) and free Citrine (∼25 kDa). The blot was then probed with anti-α-tubulin to confirm that equal amounts of protein had been loaded for each Supplementary sample. Overall, there is good correlation between the presence of MUM2-Citrine fluorescence in the mucilage pocket, and MUM2-Citrine protein on the western blot. As MUM2-Citrine was

detected in other tissues, we also imaged whole seeds at 7, 8, 9, and 10 DPA to confirm that the majority of the fluorescence is in the seed coat and not other seed tissues (Figure S2). Given that Citrine is relatively stable under a variety of conditions (Griesbeck et al., 2001) including the low pH of the vacuole (Figure 3), it is likely that the loss of fluorescence in the pocket at 9 DPA is caused by protein
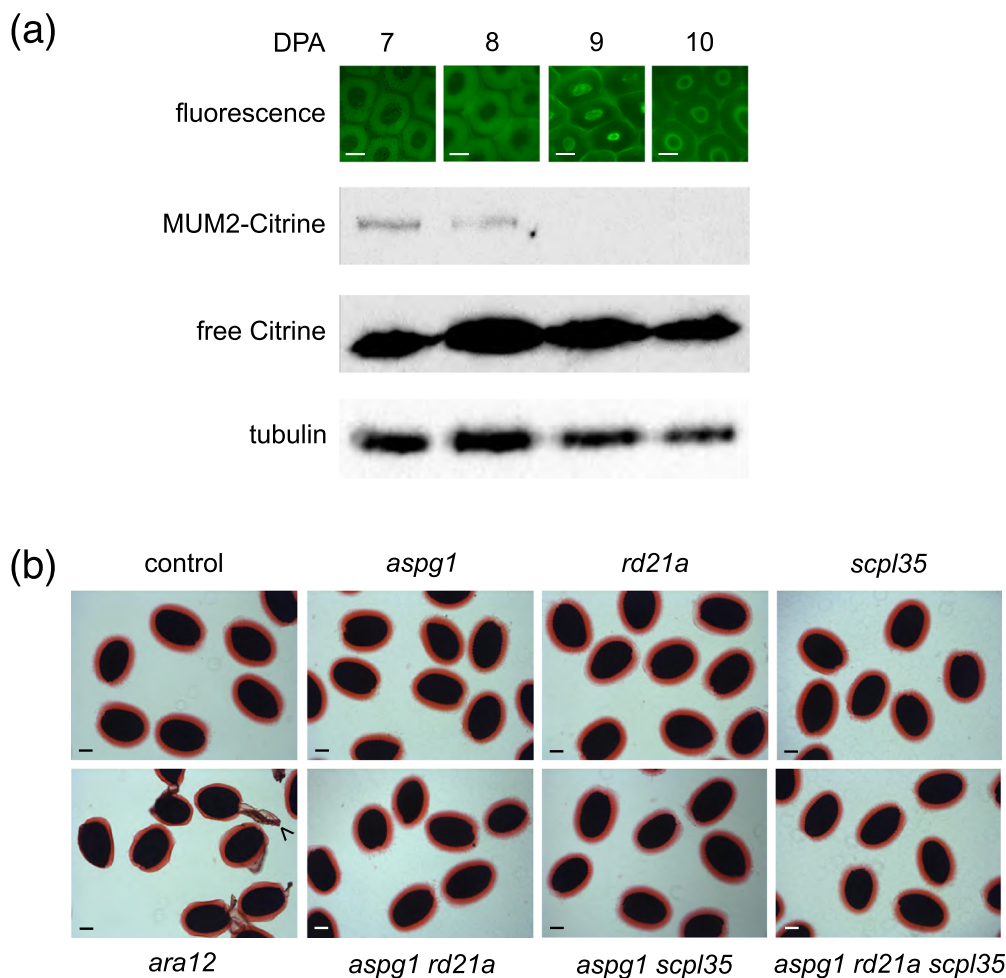
FIGURE 4 Changes in MUM2-Citrine abundance during differentiation of seed coat epidermal cells and mucilage extrusion phenotypes in protease mutants. (a) Correlation between MUM2-Citrine amounts and fluorescence in the mucilage pocket during seed coat development. Seeds from developing siliques were examined at 7, 8, 9, and 10 DPA (top row). Fluorescence is observed in the mucilage pocket at 7 and 8 DPA but disappears at 9 and 10 DPA. Total protein was extracted from the remainder of seeds from the same silique and analyzed by Western blotting. Full length MUM2-Citrine protein is only detected at 7 and 8 DPA, and free Citrine also decreases at 9 and 10 DPA. Tubulin protein was used as a loading control and is detected at all time points. Scale bar = 20 μm. (b) Mature seeds carrying mutations in the proteases *aspg1*, *rd21a*, *scpl35*, *ara12*, *aspg1 rd21a*, *aspg1 scpl35*, and *aspg1 rd21a scpl35* and the control *gMUM2-Citrine* were hydrated in water and then stained with ruthenium red to visualize extruded mucilage. The arrowhead in the *ara12* panel indicates the detached primary cell wall. Scale bar in b = 100 μm

degradation rather than loss of Citrine fluorescence due to changes in the apoplast environment.

3.6 | The proteases of the seed mucilage proteome do not influence mucilage adherence

The simplest hypothesis for the rapid decrease in MUM2-Citrine protein at 9 DPA is that it is degraded by one or more proteases. Proteomic analysis of extruded mucilage from mature seeds detected four proteases: ASPARTIC PROTEASE IN GUARD CELL 1 (ASPG1), RESPONSIVE TO DEHYDRATION 21A (RD21A), SERINE CARBOXYPEPTIDASE_LIKE 35 (SCPL35), and ARABIDOPSIS SUBTILISIN PROTEASE 12 (ARA12; Tsai et al., 2017). ARA12, also called AtSBT1.7, may be involved degradation of PMEI, and *ara12* mutants have a mucilage defect (Rautengarten et al., 2008). To determine if

any of these proteases were involved in the degradation of MUM2, lines expressing *gMUM2-Citrine* that were also homozygous for a loss-of-function mutation for one or more of these four proteases were constructed.

Extrusion of mucilage from mature seeds of the single mutants *aspg1-1*, *rd21a-2*, *scpl35-1*, *ara12-1*, double mutants *aspg1-1 rd21a-2* and *aspg1-1 scpl35-1*, and the triple mutant *aspg1-1 rd21a-2 scpl35-1* was examined. When seeds were hydrated in water without shaking, and then stained with ruthenium red, the mucilage phenotypes of the protease mutants looked very similar to that of the *gMUM2-Citrine* control except for *ara12*, which has a previously characterized mucilage extrusion phenotype where the mucilage halo is smaller than wild type, and the primary cell wall detaches from the seed (Figure S3; Rautengarten et al., 2008). When seeds were hydrated by shaking in water for 2 h and then stained with ruthenium red, the *ara12* phenotype was also apparent (Figure 4b, arrowhead indicates detached

primary cell wall). Although the *scpl35*, *rd21a* and *aspg1* single mutant halos still appeared comparable to the *gMUM2-Citrine* control, the *aspg1 rd21a*, *aspg1 scpl35*, and *aspg1 rd21a scpl35* mutant seeds appeared to have slightly smaller adherent mucilage halos (Figure 4b). As the putative extruded mucilage phenotypes were very subtle, the areas of the mucilage halos and the seeds were measured after shaking seeds in water and then staining with ruthenium red for all genotypes apart from *ara12*. Two independent sets of seed grown at different times were generated and used for analysis. Although there was variation between the control seeds (gMUM2-Citrine in *mum2-1*) and some genotypes for both seed area and seed mucilage halo area, no consistent, statistically-significant differences were observed (data not shown).

To determine whether there were macroscopic differences in the glucan structure in extruded mucilage structure, seeds were hydrated in water and then stained with calcofluor white to allow the cellulosic rays in the extruded mucilage to be visualized, but no difference was observed (Figure S4).

3.7 | Disappearance of MUM2-Citrine signal in the mucilage pocket is not significantly delayed in protease mutants

In order to determine whether MUM2 is degraded by ASPG1, RD21A, SCPL35 and ARA12, developing seeds of wild type and protease single mutants *aspg1*, r*d21a*, *scpl35*, *ara12*, double mutants *aspg1 rd21a* and *aspg1 scpl35*, and the triple mutant *aspg1 rd21a scpl35* expressing MUM2-Citrine were examined using confocal microscopy. As described previously for 9 DPA wild-type seeds (Figure 1), the secondary cell wall (columella) is just becoming visible at the same time as the fluorescent signal from MUM2-Citrine is lost from the mucilage pocket. Therefore, appearance of the secondary cell wall was used to confirm that 9 DPA siliques identified by marking open flowers as described above were indeed at the correct developmental stage. The timing of development of all single and higher order protease mutants was comparable to *gMUM2-Citrine* in *mum2*, and at 7 DPA, strong signal was observed in the mucilage pockets of all lines (Figure 5). As expected, in wild type at 9 DPA when the secondary cell wall was visible in bright-field microscopy, MUM2-Citrine fluorescence was absent from the mucilage pocket and observed in the developing secondary cell wall (Figure 5). Examination of all mutant lines failed to reveal any clear persistence of the MUM2-Citrine signal in the mucilage pocket at 9 DPA (Figure 5).

3.8 | The temporal and spatial distribution of four mucilage proteases in seed coat epidermal cells is not consistent with a role in MUM2 degradation at the end of mucilage biosynthesis

To further understand whether proteases might be involved in degradation of MUM2, the distribution patterns of ASPG1, RD21A, SCPL35, and ARA12 proteins were examined.

Genomic sequences of *ASPG1*, *RD21A*, and *SCPL35* including coding regions and 1.7, 2, and 1.4 kb of upstream sequence, respectively, were fused with mRFP. *gASPG1-mRFP*, *gRD21A-mRFP*, and *gSCPL35-mRFP* constructs were used to transform *aspg1*, *rd21a* and *scpl35* mutant lines carrying *gMUM2-Citrine* in *mum2-1* respectively, and distribution of fluorescence was determined by confocal microscopy. Due to the lack of phenotypes in these mutants as described above, complementation of the protease-mRFP constructs in the mutant background could not be assessed.

In plants expressing *gRD21a-mRFP* and *gMUM2-Citrine*, the fluorescent signal of RD21A-mRFP was detected at 7 DPA but was absent in the mucilage pocket and instead was strongest in the basal half of the cell (Figure 6a). The distribution pattern of RD21A-mRFP is distinct from the pattern of cytosolic Citrine, which is concentrated in the cytoplasmic column rather than at the base of the cell (Figure 2h). The size and position of RD21A-mRFP accumulation corresponds to that of the large vacuole of seed coat epidermal cells (Young et al., 2008). At 9 DPA, mRFP fluorescence signal was still detected predominantly in the vacuole (Figure 6b). The pattern of MUM2-Citrine fluorescence was similar to that seen in seeds expressing MUM2-Citrine alone, with strong fluorescence in the mucilage pocket at 7 DPA followed by a loss of signal in the mucilage and appearance in the developing secondary cell wall at 9 DPA (Figure 6b). The overlaid image of the distribution of RD21A-mRFP and MUM2-Citrine shows that RD21A-mRFP and MUM2-Citrine were predominantly confined to two different compartments at both 7 and 9 DPA (Figure 6).

Although microarray data indicate that *ASPG1* is expressed in seed coats (Dean et al., 2011), mRFP signal could not be detected in the epidermis of developing seed coats in plants carrying *gASPG1-mRFP* and *gMUM2-Citrine* but could be detected in the vacuole-like organelle in underlying palisade cells (data not shown). To ensure expression in the epidermal layer of the seed coat during development, a *cASPG1-mRFP* construct was generated where the *ASPG1* coding sequence was fused to *mRFP* under control of the *TBA2p* promoter, which drives strong expression in the epidermal layer of the seed coat during development (Tsai et al., 2017). Developing seed coat epidermal cells expressing ASPG1-mRFP and MUM2-Citrine were examined. The fluorescence pattern of cASPG1-mRFP was very similar to that of RD21A-mRFP, with strong expression in the vacuole at both 7 and 9 DPA (Figure 6). As before, MUM2-Citrine was observed in the mucilage pocket at 7 DPA, and disappeared from the pocket but was visible in the secondary cell wall at 9 DPA (Figure 6).

We cannot eliminate the possibilities that small amounts of RD21a-mRFP and ASPG1-mRFP may be released from the vacuole at 9 DPA and contribute to disappearance of the MUM2-Citrine signal in the mucilage pocket, or whether processing of RD21A-mRFP or cASPG1-mRFP is required for their activation in the mucilage pocket at 9 DPA and may be impaired by the fusion of mRFP to these proteins. However, as most of the RD21A-mRFP and ASPG1-mRFP signal remains in the vacuole at 9 DPA, and MUM2-Citrine signal does not appear to persist past 9 DPA in *rd21a* or *aspg1* mutant seed coat

FIGURE 5 MUM2-Citrine fluorescence patterns in protease mutant seed coat epidermal cells. MUM2-Citrine fluorescence was examined using confocal microscopy in the proteases *aspg1*, *rd21a*, *scpl35*, *ara12*, *aspg1 rd21a*, *aspg1 scpl35*, and *aspg1 rd21a scpl35* and the control *gMUM2-Citrine* in mum2. At 7 DPA, MUM2-Citrine fluorescence is observed in the mucilage pocket in all genotypes. At 9 DPA, the signal in the mucilage pocket disappears, but is visible in the developing secondary cell wall (arrow) in the *gMUM2-Citrine* control. The fluorescence also disappears in mucilage pocket of all protease mutants. Developmental stage was confirmed by presence of the developing secondary cell wall. Labels in top row are m = mucilage pocket, cc = cytoplasmic column, and arrow in 9 DPA images = secondary cell wall. These features are observed in all subsequent panels but are not labeled. All images were taken at the same magnification. Scale bar = 25 μm
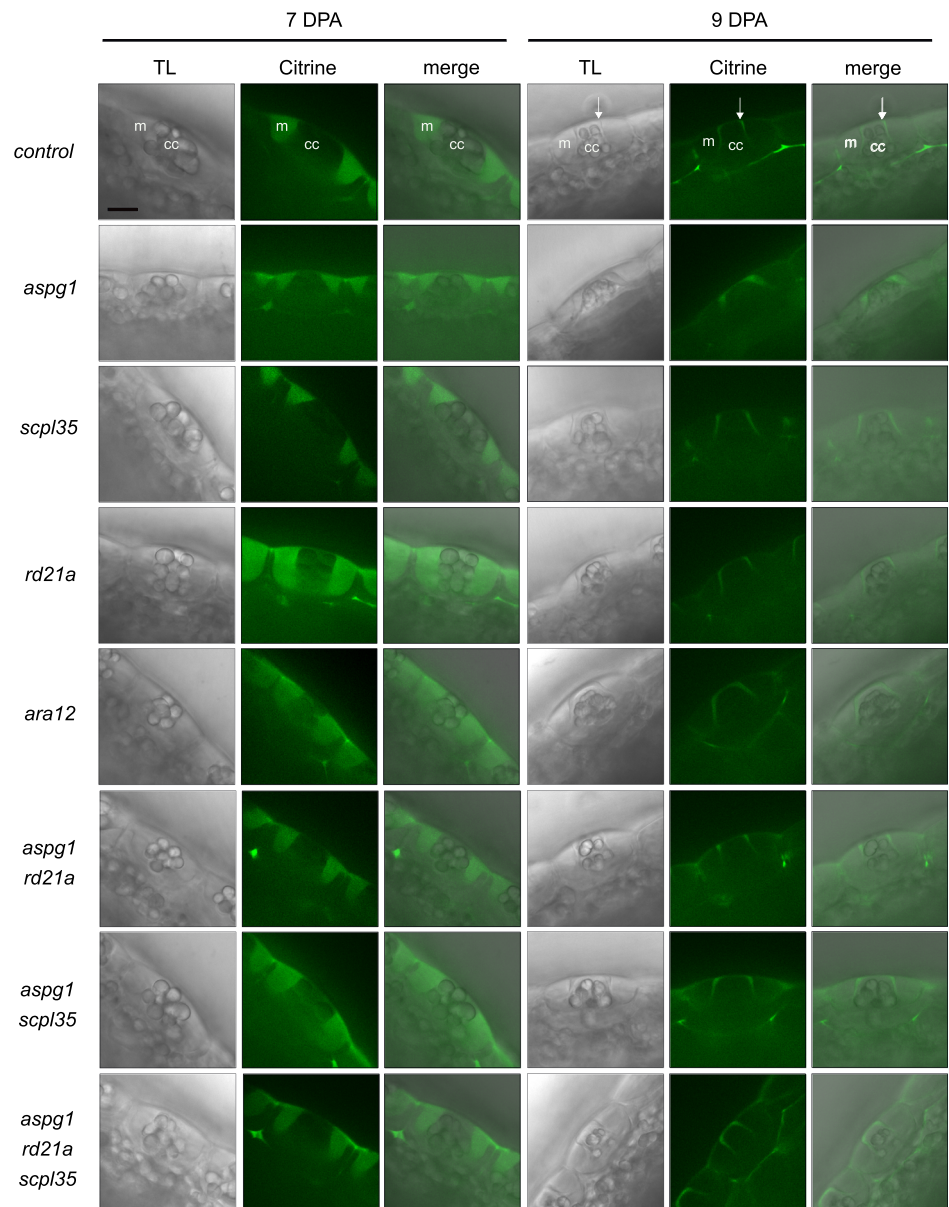
epidermal cells (Figure 5), we favor the hypothesis that RD21a and ASPG1 are not major proteases involved in MUM2-Citrine degradation.

SCPL35-mRFP was observed in the mucilage pocket and primary cell walls at 7 DPA and remained in the pocket at 9 DPA (Figure 6) in plants expressing both *gSCPL35-mRFP* and *gMUM2-Citrine*. As SCPL35 and MUM2 were co-localized in the mucilage pocket when fluorescent signal of MUM2-Citrine was detectable at 7 DPA, and MUM2-Citrine signal does not appear to persist past 9 DPA in *scpl35* mutants (Figure 5), it does not seem likely that SCPL35 is involved in the degradation of MUM2-Citrine.

Previously in our lab, the *ARA12* genomic sequence, including 3.2 kb of upstream sequence and the coding region fused to mRFP, was shown to be unable to complement the *ara12* phenotype (data not shown). Therefore, the *ARA12* coding sequence was fused to *mRFP* under the control of the *TBA2* promoter and introduced into *ara12* mutant plants carrying *gMUM2-Citrine*. Of 12 independent transgenic lines, four showed complementation of the *ara12* seed coat phenotype when mature seeds were hydrated by shaking in water and then stained in ruthenium red (Figure S5). Detachment of the primary cell wall was not observed but less mucilage was extruded in comparison to wild type. Developing seed from these complemented lines was examined analyzed using confocal microscopy. Both MUM2-Citrine and ARA12-mRFP fluorescence were detected in the mucilage pocket at 7 DPA (Figure 6A). At 9 DPA, MUM2-Citrine was no longer observed in the mucilage pocket, whereas ARA12-mRFP fluorescence persisted (Figure 6b). Like SCPL35-RFP, given that MUM2-Citrine fluorescence co-localizes with ARA12-mRFP in the mucilage pocket at 7 DPA, and that MUM2-Citrine fluorescence does not persist in *ara12* mutant mucilage pockets at 9 DPA (Figure 5), it does not seem likely that ARA12 is primarily responsible for degrading MUM2-Citrine at 9 DPA.
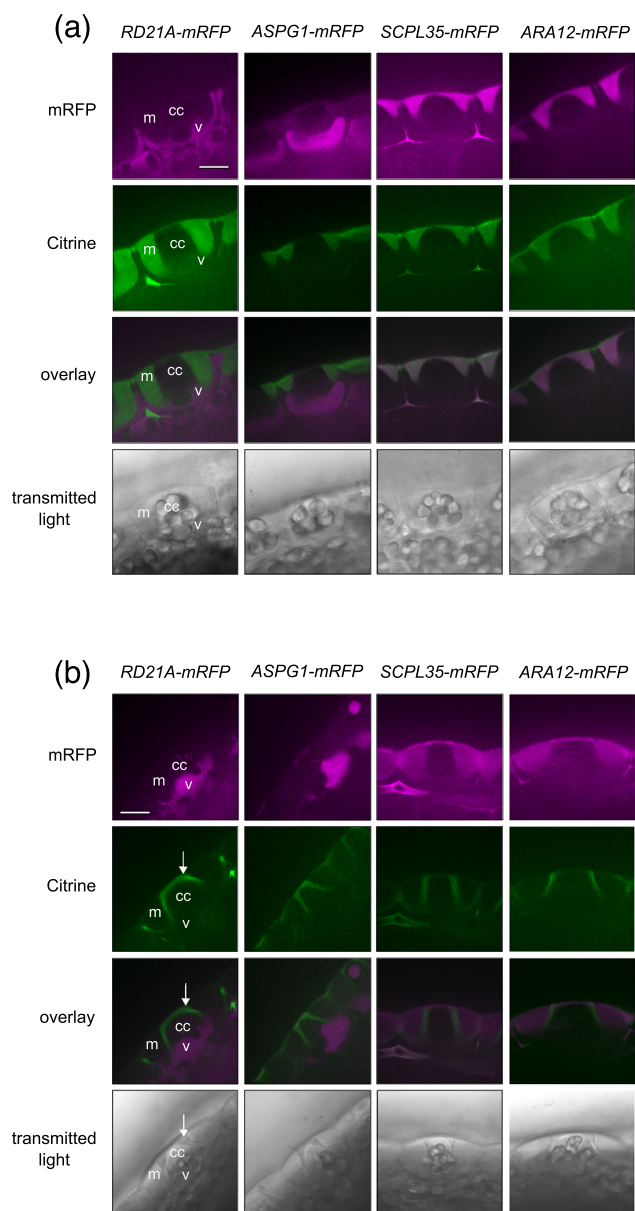
FIGURE 6 Protease-mRFP and MUM2-Citrine fluorescence patterns in seed coat epidermal cells. Seed coat epidermal cells expressing protease-mRFP fusion proteins and MUM2-Citrine were examined using confocal microscopy. (a) At 7 DPA, MUM2-Citrine fluorescence is located in the apoplastic mucilage pocket in all transgenic lines. Both RD21A-mRFP and ASPG1-mRFP fluorescence is predominantly located in the vacuole, while SCPL35-mRFP and ARA12-mRFP signal is co-localized with MUM2-Citrine in the mucilage pocket. (b) At 9 DPA, developmental stage was confirmed by the presence of the developing secondary cell wall (arrow, first column but visible in all bright-field panels). MUM2-Citrine fluorescence has disappeared from the mucilage pocket in all transgenic lines. mRFP fluorescence remains predominantly in the vacuole in RD21A-mRFP- and ASPG1-mRFP-expressing cells, and in the mucilage pocket in cells expressing SCPL35-mRFP and ARA12-RFP. Labels in first column are m = mucilage pocket, cc = cytoplasmic column, v = vacuole. These features are observed in all subsequent panels but are not labeled. All images were taken at the same magnification. Scale bar = 25 μm

4 | DISCUSSION

We have shown that the distribution of the cell wall protein MUM2 in seed coat epidermal cells is distributed in a polar manner, accumulating in the mucilage pocket as it expands from 5 to 8 DPA. The polar distribution of MUM2 is cell type-specific since its localization in other cell types is more evenly distributed in the apoplast. Other seed coat epidermal proteins secreted to the apoplast during mucilage synthesis that have been examined to date, including PER36 (Kunieda et al., 2013), three cellulose synthases CESA3, CESA5, CESA10 (Griffiths et al., 2015), three mucilage proteins of unknown function, TBA1, TBA2, and TBA3 (Tsai et al., 2017), PRX50 (Francoz et al., 2019) and VAMP721 and VAMP722 (this study) are also distributed asymmetrically, either in the mucilage pocket (TBA1, TBA2, TBA3, PRX50), the plasma membrane lining the mucilage pocket (CESA3, CESA5, CESA10, VAMP721, VAMP722) or the portion of the primary cell wall surrounding the pocket (PER36). Further, the chimeric protein secCitrine shows a similar polarized pattern of distribution in seed coat epidermal cells, indicating that the asymmetry is not determined by the amino acid sequence of the cargo. Finally, the asymmetry of so many secreted proteins and polysaccharides, regardless of whether their final destination is the plasma membrane, cell wall or mucilage pocket, as well as the fact that two of the asymmetric proteins are v-SNAREs, suggests that the asymmetry occurs via targeted secretion. Taken together, these data suggest that seed coat epidermal cells redirect secretion prior to the deposition of mucilage, such that secretory vesicles are targeted to the future site of the mucilage pocket. The mechanism that controls this targeting is not yet identified. However, since seed coat epidermal cell development is well characterized, is asymmetric without involving the complications of cell growth, and is amenable to genetic analyses, it has potential as a relatively simple but powerful model system for investigating the cellular and biochemical mechanisms of polar secretion.

Unexpectedly, we observed that MUM2-Citrine protein fluorescence abruptly disappears from the entire pocket between 8 and 9 DPA. The fluorescence of other YFP- or RFP-tagged proteins associated with the mucilage pocket including TBA1, TBA 2, TBA3, and PRX50 also seems to disappear at a similar time (Francoz et al., 2019; Tsai et al., 2017). The loss of MUM2-Citrine fluorescence at this stage in development is correlated with a reduction in MUM2-Citrine protein levels as detected using western blots implying that the observed changes are due to protein degradation rather than simply a reduction in fluorescence of the fluorophore. Thus, it is possible that the entire mucilage proteome is at least partially degraded at this developmental stage.

The mechanism underlying the decrease in the mucilage proteome is unclear. It coincides with the end of mucilage synthesis and the beginning of columellae synthesis, which presumably prevents further secretion to the mucilage pocket by forming a physical barrier. It is possible that the abrupt decrease in mucilage-associated proteins is not due to an increase in degradation but rather a decrease in their synthesis and/or deposition combined with constant protein turnover. Alternatively, the abrupt decrease in mucilage proteome at 9 DPA could be due to both a decrease in synthesis and an increase in the

degradation. The fact that MUM2-Citrine is distributed evenly in the mucilage pocket during differentiation, rather than forming a gradient with the highest concentration at the site of deposition just outside the plasma membrane and the lowest concentration near the primary cell wall, suggests that protein turnover is not continuous during mucilage synthesis but occurs abruptly throughout the entire mucilage pocket at the end of this developmental stage.

We investigated whether four different proteases identified in the mature mucilage proteome (Tsai et al., 2017) might be involved in the decrease in MUM2-Citrine. However, as the temporal and spatial distribution of these proteases do not coincide with the degradation of MUM2-Citrine in the apoplast, and loss of the proteases alone or in combination failed to decrease MUM2 degradation, it does not appear that these proteases are the major effectors of MUM2-Citrine degradation. It is possible that the quadruple combination of mutations (e.g., *aspg1 rd21a scpl35 ara12*) is necessary to abolish proteome degradation, or that other, as yet unidentified proteases exist in the mucilage.

Since mutants that fail to degrade MUM2-Citrine have not been identified, the role of the disappearance remains unknown. It is possible that the abrupt removal of carbohydrate-active proteins, like MUM2, limits their activity and influences mucilage structure and function. Alternatively, the degradation and reabsorption of the resulting peptides might represent an amino acid salvage pathway for the seed coat epidermal cells. The investigation of such hypotheses depends on the identification of mutants that fail to degrade MUM2-Citrine at the end of mucilage synthesis.

It has been suggested that myxospermous species could be engineered such that valuable recombinant proteins are deposited in the mucilage pocket. Such proteins could then be harvested from intact mature seed simply by exposing the seed to water and extracting the mucilage (Dean et al., 2017; Francoz et al., 2018). The discovery that the mucilage proteome may be degraded at the end of mucilage synthesis would prevent such an application until methods that prevent the degradation can be identified.

CONFLICT OF INTEREST

The Authors did not report any conflict of interest.

AUTHOR CONTRIBUTIONS

Y.-C.L., G.H.D., and G.W.H. designed experiments, analyzed data, and wrote the manuscript. Y-C.L., G.H.D., E.G., and A.Y.-L.T. performed experiments.

DATA AVAILABILITY STATEMENT

All data supporting the findings of this study are available within the paper and the supplementary data published online.

ORCID

Yi-Chen Lee https://orcid.org/0000-0003-0607-9410
Gillian H. Dean https://orcid.org/0000-0003-1126-8355
Erin Gilchrist https://orcid.org/0000-0002-9232-6504
Allen Yi-Lun Tsai https://orcid.org/0000-0002-4232-2281
George W. Haughn https://orcid.org/0000-0001-8164-8826

REFERENCES

Alonso, J. M., Stepanova, A. N., Leisse, T. J., Kim, C. J., Chen, H., Shinn, P., Stevenson, D. K., Zimmerman, J., Barajas, P., Cheuk, R., & Gadrinab, C. (2003). Genome-wide insertional mutagenesis of *Arabidopsis thaliana*. *Science (New York, N.Y.)*, *301*, 653–657.

Armenteros, J. J. A., Tsirigos, K. D., Sønderby, C. K., Petersen, T. N., Winther, O., Brunak, S., von Heijne, G., & Nielsen, H. (2019). SignalP 5.0 improves signal peptide predictions using deep neural networks. *Nature Biotechnology*, *37*, 420–423. https://doi.org/10.1038/s41587-019-0036-z

Batoko, H., Zheng, H. Q., Hawes, C., & Moore, I. (2000). A Rab1 GTPase is required for transport between the endoplasmic reticulum and Golgi apparatus and for normal Golgi movement in plants. *Plant Cell*, *12*, 2201–2217. https://doi.org/10.1105/tpc.12.11.2201

Beeckman, T., De Rycke, R., Viane, R., & Inzé, D. (2000). Histological study of seed coat development in *Arabidopsis thaliana*. *Journal of Plant Research*, *113*, 139–148. https://doi.org/10.1007/PL00013924

Bove, J., Vaillancourt, B., Kroeger, J., Hepler, P. K., Wiseman, P. W., & Geitmann, A. (2008). Magnitude and direction of vesicle dynamics in growing pollen tubes using spatiotemporal image correlation spectroscopy and fluorescence recovery after photobleaching. *Plant Physiology*, *147*, 1646–1658. https://doi.org/10.1104/pp.108.120212

Chung, M.-H., Chen, M.-K., & Pan, S.-M. (2000). Floral spray transformation can efficiently generate Arabidopsis transgenic plants. *Transgenic Research*, *9*, 471–486. https://doi.org/10.1023/A:1026522104478

Dean, G. H., Cao, Y., Xiang, D., Provart, N. J., Ramsay, L., Ahad, A., White, R., Selvaraj, G., Datla, R., & Haughn, G. W. (2011). Analysis of gene expression patterns during seed coat development in *Arabidopsis*. *Molecular Plant*, *4*, 1074–1091. https://doi.org/10.1093/mp/ssr040

Dean, G. H., Jin, Z., Shi, L., Esfandiari, E., McGee, R., Nabata, K., Lee, T., Kunst, L., Western, T. L., & Haughn, G. W. (2017). Identification of a seed coat-specific promoter fragment from the Arabidopsis *MUCILAGE-MODIFIED4* gene. *Plant Molecular Biology*, *95*, 33–50. https://doi.org/10.1007/s11103-017-0631-7

Dean, G. H., Zheng, H., Tewari, J., Huang, J., Young, D. S., Hwang, Y. T., Western, T. L., Carpita, N. C., McCann, M., Mansfield, S. D., & Haughn, G. W. (2007). The *Arabidopsis* MUM2 gene encodes a β-galactosidase required for the production of seed coat mucilage with correct hydration properties. *Plant Cell*, *19*, 4007–4021. https://doi.org/10.1105/tpc.107.050609

DeBono, A. G. (2011). The role and behavior of *Arabidopsis thaliana* lipid transfer proteins during cuticular wax deposition. PhD thesis, University of British Columbia. https://open.library.ubc.ca/cIRcle/collections/ubctheses/24/items/1.0072411. Accessed June 2021.

Dittman, J. S., & Kaplan, J. M. (2006). Factors regulating the abundance and localization of synaptobrevin in the plasma membrane. *Proceedings of the National Academy of Sciences*, *103*, 11399–11404. https://doi.org/10.1073/pnas.0600784103

Francoz, E., Lepiniec, L., & North, H. M. (2018). Seed coats as an alternative molecular factory: Thinking outside the box. *Plant Reproduction*, *31*, 327–342. https://doi.org/10.1007/s00497-018-0345-2

Francoz, E., Ranocha, P., Le Ru, A., Martinez, Y., Fourquaux, I., Jauneau, A., Dunand, C., & Burlat, V. (2019). Pectin demethylesterification generates platforms that anchor peroxidases to remodel plant cell wall domains. *Developmental Cell*, *48*, 261–276. https://doi.org/10.1016/j.devcel.2018.11.016

Gendre, D., McFarlane, H. E., Johnson, E., Mouille, G., Sjodin, A., Oh, J., Levesque-Tremblay, G., Watanabe, Y., Samuels, L., & Bhalerao, R. P. (2013). *Trans*-golgi network localized ECHIDNA/Ypt interacting protein complex is required for the secretion of cell wall polysaccharides in *Arabidopsis*. *Plant Cell*, *25*, 2633–2646. https://doi.org/10.1105/tpc.113.112482

Gendre, D., Oh, J., Boutté, Y., Best, J. G., Samuels, L, Nilsson, R., Uemura, T., Marchant, A., Bennett, M. J., Grebe, M., & Bhalerao, R. P. (2011). Conserved *Arabidopsis* ECHIDNA protein mediates *trans*–Golgi-network trafficking and cell elongation. *Proceedings of the National Academy of Sciences*, *108*, 8048–8053. https://doi.org/10.1073/pnas.1018371108

Griesbeck, O., Baird, G. S., Campbell, R. E., Zacharias, D. A., & Tsien, R. Y. (2001). Reducing the environmental sensitivity of yellow fluorescent protein. *Journal of Biological Chemistry*, *276*, 29188–29194. https://doi.org/10.1074/jbc.M102815200

Griffiths, J. S., Šola, K., Kushwaha, R., Lam, P., Tateno, M., Young, R., Voiniciuc, C., Dean, G., Mansfield, S. D., DeBolt, S., & Haughn, G. W. (2015). Unidirectional movement of cellulose synthase complexes in Arabidopsis seed coat epidermal cells deposit cellulose involved in mucilage extrusion, adherence, and ray formation. *Plant Physiology*, *168*, 502–520. https://doi.org/10.1104/pp.15.00478

Haughn, G. W., & Somerville, C. (1986). Sulfonylurea-resistant mutants of *Arabidopsis thaliana*. *Molecular and General Genetics*, *204*, 430–434. https://doi.org/10.1007/BF00331020

Haughn, G. W., & Western, T. L. (2012). *Arabidopsis* seed coat mucilage is a specialized cell wall that can be used as a model for genetic analysis of plant cell wall structure and function. *Frontiers in Plant Science*, *3*, 1–5.

Hellens, R. P., Edwards, E. A., Leyland, N. R., Bean, S., & Mullineaux, P. M. (2000). pGreen: A versatile and flexible binary Ti vector for agrobacterium-mediated plant transformation. *Plant Molecular Biology*, *42*, 819–832. https://doi.org/10.1023/A:1006496308160

Ichikawa, M., Hirano, T., Enami, K., Fuselier, T., Kato, N., Kwon, C., Voigt, B., Schulze-Lefert, P., Baluška, F., & Sato, M. H. (2014). Syntaxin of plant proteins SYP123 and SYP132 mediate root hair tip growth in *Arabidopsis thaliana*. *Plant and Cell Physiology*, *55*, 790–800. https://doi.org/10.1093/pcp/pcu048

Kleinboelting, N., Huep, G., Kloetgen, A., Viehoever, P., & Weisshaar, B. (2012). GABI-Kat SimpleSearch: New features of the *Arabidopsis thaliana* T-DNA mutant database. *Nucleic Acids Research*, *40*, 1211–1215.

Kost, B. (2008). Spatial control of rho (Rac-Rop) signaling in tip-growing plant cells. *Trends in Cell Biology*, *18*, 119–127. https://doi.org/10.1016/j.tcb.2008.01.003

Kunieda, T., Shimada, T., Kondo, M., Nishimura, M., Nishitani, K., & Hara-Nishimura, I. (2013). Spatiotemporal secretion of PEROXIDASE36 is required for seed coat mucilage extrusion in *Arabidopsis*. *The Plant Cell*, *25*, 1355–1367. https://doi.org/10.1105/tpc.113.110072

Kwon, C., Neu, C., Pajonk, S., Yun, H. S., Lipka, U., Humphry, M., Bau, S., Straus, M., Kwaaitaal, M., Rampelt, H., Kasmi, F. E., Jürgens, G., Parker, J., Panstruga, R., Lipka, V., & Schulze-Lefert, P. (2008). Co-option of a default secretory pathway for plant immune responses. *Nature*, *451*, 835–841. https://doi.org/10.1038/nature06545

Laemmli, U. K. (1970). Cleavage of structural proteins during the assembly of the head of bacteriophage T4. *Nature*, *227*, 680–685. https://doi.org/10.1038/227680a0

Lancelle, S. A., & Hepler, P. K. (1992). Ultrastructure of freeze-substituted pollen tubes of *Lilium longiflorum*. *Protoplasma*, *167*, 215–230. https://doi.org/10.1007/BF01403385

Lu, Q. S., Dela Paz, J., Pathmanathan, A., Chiu, R. S., Tsai, A. Y.-L., & Gazzarrini, S. (2010). The C-terminal domain of FUSCA3 negatively regulates mRNA and protein levels, and mediates sensitivity to the hormones abscisic acid and gibberellic acid in Arabidopsis. *The Plant Journal*, *64*, 100–113. https://doi.org/10.1111/j.1365-313X.2010.04307.x

Macquet, A., Ralet, M.-C., Loudet, O., Kronenberger, J., Mouille, G., Marion-Poll, A., & North, H. M. (2007). A naturally occurring mutation in an *Arabidopsis* accession affects a β-D-galactosidase that increases the hydrophilic potential of rhamnogalacturonan I in seed mucilage. *Plant Cell*, *19*, 3990–4006. https://doi.org/10.1105/tpc.107.050179

McFarlane, H. E., Watanabe, Y., Gendre, D., Carruthers, K., Levesque-Tremblay, G., Haughn, G. W., Bhalerao, R. P., & Samuels, L. (2013). Cell wall polysaccharides are mislocalized to the vacuole in *echidna* mutants. *Plant and Cell Physiology*, *54*, 1867–1880. https://doi.org/10.1093/pcp/pct129

McGee, R., Dean, G. H., Mansfield, S. D., & Haughn, G. W. (2019). Assessing the utility of seed coat-specific promoters to engineer cell wall polysaccharide composition of mucilage. *Plant Molecular Biology*, *101*, 373–387. https://doi.org/10.1007/s11103-019-00909-8

McGee, R., Dean, G. H., Wu, D., Zhang, Y., Mansfield, S. D., & Haughn, G. W. (2021). Pectin modification in seed coat mucilage by in vivo expression of rhamnogalacturonan-I- and homogalacturonan-degrading enzymes. *Plant and Cell Physiology*, pcab077. https://doi.org/10.1093/pcp/pcab077

Nakagawa, T., Ishiguro, S., & Kimura, T. (2009). Gateway vectors for plant transformation. *Plant Biotechnology*, *26*, 275–284. https://doi.org/10.5511/plantbiotechnology.26.275

Nakagawa, T., Nakamura, S., Tanaka, K., Kawamukai, M., Suzuki, T., Nakamura, K., Kimura, T., & Ishiguro, S. (2008). Development of R4 gateway binary vectors (R4pGWB) enabling high-throughput promoter swapping for plant research. *Bioscience, Biotechnology, and Biochemistry*, *72*, 624–629. https://doi.org/10.1271/bbb.70678

Oshima, Y., Mitsuda, N., Nakatam, M., Nakagawa, T., Nagaya, S., Kato, K., & Ohme-Takagi, M. (2011). Novel vector systems to accelerate functional analysis of transcription factors using chimeric repressor gene-silencing technology (CRES-T). *Plant Biotechnology*, *28*, 201–210. https://doi.org/10.5511/plantbiotechnology.11.0124a

Qi, J., & Greb, T. (2017). Cell polarity in plants: The yin and Yang of cellular functions. *Current Opinion in Plant Biology*, *35*, 105–110. https://doi.org/10.1016/j.pbi.2016.11.015

Rautengarten, C., Usadel, B., Neumetzler, L., Hartmann, J., Büssis, D., & Altmann, T. (2008). A subtilisin-like serine protease essential for mucilage release from Arabidopsis seed coats. *The Plant Journal*, *54*, 466–480. https://doi.org/10.1111/j.1365-313X.2008.03437.x

Rounds, C. M., & Bezanilla, M. (2013). Growth mechanisms in tip-growing plant cells. *Annual Review of Plant Biology*, *64*, 243–265. https://doi.org/10.1146/annurev-arplant-050312-120150

Samuels, L., Kunst, L., & Jetter, R. (2008). Sealing plant surfaces: Cuticular wax formation by epidermal cells. *Annual Review of Plant Biology*, *59*, 683–707. https://doi.org/10.1146/annurev.arplant.59.103006.093219

Sanderfoot, A. A., Assaad, F. F., & Raikhel, N. V. (2000). The Arabidopsis genome. An abundance of soluble *N*-ethylmaleimide-sensitive factor adaptor protein receptors. *Plant Physiology*, *124*, 1558–1569. https://doi.org/10.1104/pp.124.4.1558

Schindelin, J., Arganda-Carreras, I., Frise, E., Kaynig, V., Longair, M., Pietzsch, T., Preibisch, S., Rueden, C., Saalfeld, S., Schmid, B., Tinevez, J. Y., White, D. J., Hartenstein, V., Eliceiri, K., Tomancak, P., & Cardona, A. (2012). Fiji: An open-source platform for biological-image analysis. *Nature Methods*, *9*, 676–682. https://doi.org/10.1038/nmeth.2019

Schuetz, M., Smith, R., & Ellis, B. E. (2013). Xylem tissue specification, patterning, and differentiation mechanisms. *Journal of Experimental Botany*, *64*, 11–31. https://doi.org/10.1093/jxb/ers287

Sessions, A., Burke, E., Presting, G., Aux, G., McElver, J., Patton, D., Dietrich, B., Ho, P., Bacwaden, J., Ko, C., Clarke, J. D., Cotton, D., Bullis, D., Snell, J., Miguel, T., Hutchison, D., Kimmerly, B., Mitzel, T., Katagiri, F., ... Goff, S. A. (2002). A high-throughput Arabidopsis reverse genetics system. *The Plant Cell*, *14*, 2985–2994. https://doi.org/10.1105/tpc.004630

Shi, L., Dean, G. H., Zheng, H., Meents, M. J., Haslam, T. M., Haughn, G. W., & Kunst, L. (2019). ECERIFERUM11/C-TERMINAL DOMAIN PHOSPHATASE-LIKE2 affects secretory trafficking. *Plant Physiology*, *181*, 901–915. https://doi.org/10.1104/pp.19.00722

Šola, K., Dean, G. H., & Haughn, G. W. (2019). Arabidopsis seed mucilage, a specialized extracellular matrix that demonstrates the structure-function versatility of cell wall polysaccharides. *Annual Plant Reviews Online*, *2*, 1085–1116.

Šola, K., Gilchrist, E. J., Ropartz, D., Wang, L., Feussner, I., Mansfield, S. D., Ralet, M.-C., & Haughn, G. W. (2019). RUBY, a putative galactose oxidase, influences pectin properties and promotes cell-to-cell adhesion in the seed coat epidermis of Arabidopsis thaliana. *The Plant Cell*, *31*, 809–831. https://doi.org/10.1105/tpc.18.00954

Tsai, A. Y.-L., Kunieda, T., Rogalski, J., Foster, L. J., Ellis, B. E., & Haughn, G. W. (2017). Identification and characterization of seed coat mucilage proteins. *Plant Physiology*, *173*, 1059–1074. https://doi.org/10.1104/pp.16.01600

Uemura, T., Ueda, T., Ohniwa, R. L., Nakano, A., Takeyasu, K., & Sato, M. H. (2004). Systematic analysis of SNARE molecules in Arabidopsis: Dissection of the post-Golgi network in plant cells. *Cell Structure and Function*, *29*, 49–65. https://doi.org/10.1247/csf.29.49

Western, T. L., Burn, J., Tan, W. L., Skinner, D. J., Martin-McCaffrey, L., Moffatt, B. A., & Haughn, G. W. (2001). Isolation and characterization of mutants defective in seed coat mucilage secretory cell development in Arabidopsis. *Plant Physiology*, *127*, 998–1011. https://doi.org/10.1104/pp.010410

Western, T. L., Skinner, D. J., & Haughn, G. W. (2000). Differentiation of mucilage secretory cells of the Arabidopsis seed coat. *Plant Physiology*, *122*, 345–356. https://doi.org/10.1104/pp.122.2.345

Windsor, J. B., Symonds, V. V., Mendenhall, J., & Lloyd, A. M. (2000). *Arabidopsis* seed coat development: Morphological differentiation of the outer integument. *Plant Journal*, *22*, 483–493. https://doi.org/10.1046/j.1365-313x.2000.00756.x

Yalovsky, S., Bloch, D., Sorek, N., & Kost, B. (2008). Regulation of membrane trafficking, cytoskeleton dynamics, and cell polarity by ROP/RAC GTPases. *Plant Physiology*, *147*, 1527–1543. https://doi.org/10.1104/pp.108.122150

Yang, K., Wang, L., Le, J., & Dong, J. (2020). Cell polarity: Regulators and mechanisms in plants. *Journal of Integrative Plant Biology*, *62*, 132–147. https://doi.org/10.1111/jipb.12904

Young, R. E., McFarlane, H. E., Hahn, M. G., Western, T. L., Haughn, G. W., & Samuels, A. L. (2008). Analysis of the Golgi apparatus in Arabidopsis seed coat cells during polarized secretion of pectin-rich mucilage. *Plant Cell*, *20*, 1623–1638. https://doi.org/10.1105/tpc.108.058842

Zhang, L., Zhang, H., Liu, P., Hao, H., Jin, J. B., & Lin, J. (2011). Arabidopsis R-SNARE proteins VAMP721 and VAMP722 are required for cell plate formation. *PLoS ONE*, *6*, e26129. https://doi.org/10.1371/journal.pone.0026129

SUPPORTING INFORMATION

Additional supporting information may be found in the online version of the article at the publisher's website.